Investigating the Performance of Grooved Heat Pipe Exposed to Constant Temperature Boundary Conditions in The Evaporator and Condenser Sections

Sajjad Ahangar Zonouzi[1], Abbas Falsafi[2], Habib Aminfar[2], Abdolhamid Azizi[1,*]

[1] *Department of Mechanical Engineering, Ilam University, Ilam, Iran.*
[2] *Faculty of Mechanical Engineering, University of Tabriz, Tabriz, Iran*
**Corresponding author: ah.azizi@ilam.ac.ir*

Manuscript received 22 July, 2024; revised 27 August, 2024; accepted 31 August, 2024. Paper no. JEMT-2407-1522.

Heat pipes have shown great potential as a technology for solving thermal management issues. They offer highly effective solutions for thermal regulation across a wide range of energy applications. One of the key novelties of this study lies in the comparative analysis of micro-grooved versus ungrooved heat pipes using a 3D transient model, which has not been extensively explored in previous research. The investigation is carried out using a 3D transient model and implementing Volume of Fluid and Lee thermal phase change models. The model's predictions align well with existing experimental data, confirming its accuracy. In this work, the effects of different evaporator temperatures and heat transfer coefficients of condenser section on heat transfer are considered. The heat transfer rate, volume fractions, temperature and velocity distribution are predicted using a 3D model for both grooved and ungrooved heat pipes. The results reveal that the grooved heat pipe significantly outperforms the ungrooved counterpart, with the heat transfer rate nearly doubling. Besides, according to the results, the addition of grooves has increased the thermal capacity of the heat pipe dramatically.

Keywords: *Grooved Heat Pipe, Numerical Modelling, Thermal Performance, Transient Behaviour*

http://dx.doi.org/ 10.22109/jemt.2024.469270.1522

1. Introduction

The efficient management and utilization of energy resources is a critical challenge facing modern society. Heat pipes have emerged as a promising technology to address this challenge, offering highly effective thermal management solutions across a wide range of energy applications. Grooved heat pipes, in particular, have garnered significant interest due to their ability to passively transport large amounts of heat with minimum temperature differential between the evaporator and condenser parts. Modern industrial heat generation devices, such as electronics and aerospace apparatus, are being designed with smaller sizes and lighter weights to accommodate technological advancements. However, this downsizing leads to higher heat output per unit area. To tackle this challenge, innovative heat transfer and dissipation tools need to be designed and analyzed to fit within smaller spaces and provide higher heat transfer efficiency. This is crucial to prevent potential damage to the heat source caused by malfunctioning heat transfer devices. Micro-grooved heat pipes (MGHPs) are widely employed in various applications, including aerospace and electronic chips in smartphones. Notably, MGHPs operate without an external power source and require minimal installation space. They exhibit higher thermal conductivity compared to their base metal counterparts. Heat pipes operate based on the mechanism of heat transfer through phase change. The liquid absorbs heat at the heat source, evaporates, and the resulting vapor moves to the heat sink section due to pressure differences. There, the vapor dissipates heat and condenses into the liquid phase and under the influence of capillary and gravitational forces, the condensate flows back to the heat source, sustaining an indefinite cycle. Among the various types of heat pipes, micro-grooved heat pipes employ certain axial grooved wicks on the inner surface. These grooves enhance the capillary drive for the condensate liquid while preserving the gravitational effect, ensuring efficient heat transfer. It should also be added that creating consistent micro-grooves requires advanced, often costly, techniques that may not be easily scaled for large-scale production. Additionally, the choice of materials must balance thermal conductivity with durability and compatibility with the working fluid. These challenges could impact the practical implementation and scalability of micro-grooved heat pipes, possibly limiting their widespread adoption to specialized or high-value applications. However, advancements in fabrication technologies and materials science could eventually mitigate these obstacles, making this technology more accessible for broader thermal management applications. The enhanced thermal performance of the micro-grooved heat pipe (MGHP) has significant potential in applications like electronics cooling, renewable energy systems, and aerospace thermal control. Its ability to improve heat dissipation and stability can lead to more efficient and reliable designs across these industries.

There are some studies in the literature about numerical modeling of heat pipes. Rouaze et al. [1] improved a one-dimensional numerical

code to simulate pulsating heat pipes. Their code simulates the dynamics of liquid slugs and vapor plugs, taking into account their interactions with the pipe walls. Heat transfer, including evaporation, condensation, and convection, is predicted using a Three-Zone Model. Jubori et al. [2] developed a two-dimensional CFD model to enhance the modleing of wickless heat pipe operation. The study investigated temperature profiles, thermal resistance, and the effects of filling ratios, inclination angles, and heat input. The results demonstrated that increasing heat input reduced thermal resistance along the WHP and highlighted the capability of the CFD model to visualize droplet dynamics and heat transfer under varying operating conditions. Tarokh et al. [3] aimed to enhance the thermal efficiency of a thermosyphon by modifying its geometry with a vortex generating obstacle. The obstacle alters the flow path, inducing a thermal boundary layer interaction that enhances convective heat transfer. A comprehensive numerical model was designed to simulate the dynamics of phase transitions and the distribution of temperature across various phases. The findings indicated that positioning the vortex generator in the adiabatic and condenser regions of the thermosyphon influenced the temperature along the thermosyphon wall. Jose et al. [4] performed a computational study on wickless heat pipes for managing electronic thermal loads. They used CuO and Al2O3 nanofluids at varying concentrations and analyzed their impact on thermal performance of the wickless heat pipes. Results showed that the nanofluids improved thermal performance, with the Al2O3 nanofluid demonstrating greater reductions in thermal resistance. The study highlights the potential of nanofluids in enhancing heat pipe efficiency for electronic cooling applications.

There are also some studies in the literature about the grooved heat pipes. Abdulshaheed et al. [5] conducted an experimental analysis on a nanoengineered heat pipe to explore the influence of filling ratio and inclination angle on its thermal performance. A hydrophilic copper oxide coating (CuO) was applied to the inner wall of the heat pipe's evaporation section. Experimental results revealed that a filling ratio of 5% offered the lowest thermal resistance of 0.019 K/W, indicating the optimal configuration among the investigated FRs (3%, 5%, 10%, and 15%). Tang et al. [6] investigated the isothermal performance of micro-grooved heat pipes used for electronic heat dissipation. Their study revealed that MGHPs in low vacuum degrees experienced greater temperature drops compared to high vacuum degrees. Extending the initial vacuum duration did not consistently boost performance. Besides, higher filling rates of the working fluid led to increased temperature variations across the evaporator and condenser. The second vacuuming process significantly influenced MGHP performance, reducing the temperature difference by nearly half. Cheng et al. [7] improved capillary flow and thermal performance in grooved heat pipes. Their experiments demonstrated a significant reduction in thermal resistance, reaching up to 92.6%, compared to untreated copper heat pipes. They developed a mathematical model using a power function to accurately predict liquid flow velocity. The model's predictions closely matched experimental results, demonstrating its validity. Naemsai et al. [8] developed a numerical model using finite element analysis to estimate the thermal resistance of a sintered-grooved wick heat pipe under non-uniform conditions. Their model was verified with experimental data, showing good agreement. Gomaa et al. [9] performed an investigation to optimize the heat transfer effectiveness of a heat pipe by varying groove ratios, working fluids, and operating conditions. The results showed that heat pipes with grooves outperformed smooth tubes by 50.6% in effectiveness. They identified the optimal design and operation settings for higher thermal performance and developed a non-dimensional experimental correlation to predict heat pipe effectiveness with a standard deviation of ±6.3%. Alijani et al. [10] experimentally investigated aluminum flat grooved heat pipes with different groove widths. They studied the effect of working fluid quantity on heat transfer effectiveness. Results showed narrower grooves improved heat transfer. An optimum operating point was identified, minimizing temperature difference. This study provided novel insights into the combined effects of groove dimensions and working fluid quantity in aluminum flat grooved heat pipes. Yao et al. [11] developed a model to investigate the heat transfer processes of evaporation and condensation in axially grooved heat pipes under small angle inclination. Their numerical simulations showed that increasing input power led to a shift from fin-film to corner-film evaporation phase. The inclination angle affected liquid return flow and the essential input power required for shifting regimes. Increasing groove aspect ratio enhanced the heat transfer capacity of the AGHP.

In summary, the primary objective of this study is to comprehensively investigate the performance of grooved heat pipes under constant temperature boundary conditions in the evaporator and condenser sections. Through a comprehensive 3D numerical modeling approach, we aim to compare the flow and heat transfer characteristics of grooved and ungrooved heat pipes, with a particular focus on their thermal capacity, temperature distribution, and fluid flow behavior. By accurately predicting temperature profiles, phase distribution, and thermal behavior, our research aims to provide valuable insights into the impact of grooves on heat pipe performance. The findings of this study have the potential to advance the understanding of heat transfer in grooved heat pipes and may have significant implications for the design and optimization of heat dissipation systems in various engineering applications.

2.Methodology

2.1 Physical model and boundary conditions

In this study, two different geometries were investigated: a cylindrical grooved heat pipe and a cylindrical wickless ungrooved heat pipe, as depicted in Fig. 1. The grooved heat pipe is designed with a series of micro-grooves on its inner surface. These grooves serve multiple functions, including increasing the effective surface area for heat transfer, promoting capillary action to enhance liquid flow, and improving the overall thermal conductivity of the system. The cylindrical micro-grooved and ungrooved heat pipes analyzed in this research are divided into three distinct regions. The first region is the evaporator section, which spans a length of L_e= 13.16mm and aims to efficiently absorb heat generated by the heat source. Adjacent to the evaporator part is the adiabatic part, denoted as L_a= 13.16mm. Finally, we have the condenser section, with a length of L_C= 23.68mm, which is responsible for effectively dissipating the absorbed heat to the surrounding environment.

Table 1 Physical properties of liquid water and water vapor

	Saturation pressure (*kPa*)	Density (kg/m^3)	Specific Heat (*J/kg.K*)	Thermal conductivity (*W/m.K*)	Viscosity (*kg/m.s*)
Liquid water	4.72	993	4180	0.61	0.000692
Water vapor	4.72	0.1	1870	0.025	0.00001

The grooves depicted in Fig. 1 have specific dimensions, with a height (h) of 0.23 mm and a width (b) of 0.11 mm. In this study, the hot end of the grooved heat pipe is subjected to a constant temperature boundary condition. Furthermore, the condenser section is regarded as being in contact with the surrounding environment and subjected to convective boundary conditions. The temperature of the surrounding environment is denoted as T_∞=283 K, and the coefficient of convective heat transfer is denoted as h_∞. For the investigated heat pipe, water is selected as the operational fluid, with a filling ratio of $\frac{V_{Liquid}}{V_{MGHP}} = 0.2$. The pressure inside both the grooved and ungrooved heat pipes is

considered to be 5 KPa, with the corresponding saturation temperature of the water under this pressure being 305K. The physical properties relevant to liquid water and water vapor used in the analysis can be found in Table 1.

Table 2 The studied cases with different T_e and h_c values applied

	T_e (K)	h $(W\,m^{-2}\,K^{-1})$
case 1	320	300
case 2	325	300
case 3	330	300
case 4	340	300
case 5	350	300
case 6	360	300
case 7	340	400
case 8	340	500
case 9	340	600

In the present paper, the impacts of two distinct variables on the heat transfer efficiency of the MGHP and ungrooved heat pipe are investigated. The initial variable is the temperature set on the evaporator section, whereas the heat transfer coefficient (HTC) in the condenser section remains fixed at h_c = 300 W m^{-2} K^{-1}, with a surrounding temperature of T_∞ = 283 K. By varying the temperature at the evaporator section, the study aims to analyze the effect of varying heat inputs on the thermal characteristics and efficiency of both the MGHP heat pipe. This investigation allows for understanding how changes in temperature affect parameters such as temperature distribution, heat transfer rates, and overall thermal efficiency. The second variable is that different values of the convective HTC for the condenser surrounding have been considered while maintaining a constant temperature of 340 K for the evaporator part (T_e).

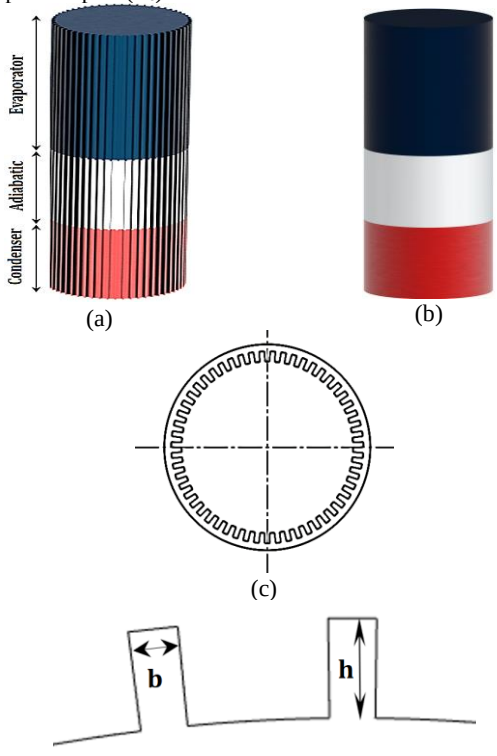

Fig. 1 Schematics of the studied problem: a) grooved heat pipe, b) ungrooved heat pipe, c) top view of the grooved heat pipe, d) geometrical parameters of the grooves

Table 2 provides an overview of the specific combinations of hc and Te values studied in the research. The HTC (h_c) represents the effectiveness of heat transfer through forced convection at the condenser surrounding, while the temperature of the evaporator section (T_e) is held constant. The table presents nine different cases, each denoted by a unique combination of h_c and T_e values. Cases 1-6 involve a coefficient of heat transfer of 300 W m^{-2} K^{-1} for the condenser surrounding, while varying the evaporator temperature (Te) from 320 K to 360 K. Cases 7-9 examine the impacts of HTC (400, 500, and 600 W m^{-2} K^{-1}) for the condenser surrounding while keeping the evaporator temperature (T_e) constant at 340 K.

2.2. Numerical approach

To obtain an approximate transient solution, the finite volume technique is used to compute numerical solutions for the time-dependent governing equations. The simulation is conducted over a duration of 15 seconds. The pressure-velocity coupling is achieved using the well-known SIMPLE algorithm. For the discretization of both the momentum and energy equations, a second-order upwind scheme is utilized. The volume fraction formulation in each simulation case is handled implicitly through the use of the implicit method. To ensure accurate calculation of volume fraction at the interface boundary cells, a compressive interface capturing technique is employed. The thresholds for achieving convergence in volume fraction and momentum residuals are set at 10^{-4}, while the energy residuals are required to achieve 10-5 at every time step. It should be added that the total number of grids in the computational domain is 202500 and the used time step size for numerical modeling of the present problem is 0.00025 s.

2.3. Governing equations

Numerical simulations of evaporation and condensation phenomena necessitate a model capable of precisely representing the behavior of a multiphase fluid. The grooved heat pipe mentioned earlier is simulated with the Volume of Fluid multiphase technique. This technique enforces the condition that the total volume fraction of all phases within each computational cell must sum up to a value of unity, as expressed in the following equation:

$$\alpha_L + \alpha_v = 1 \tag{1}$$

where α_v and α_l represent the volumetric fractions of the vapor phase and liquid phase, respectively. In this formulation, a cell with $\alpha_v = 1$ indicates that the cell is completely filled with vapor, and a cell with $\alpha_l = 1$ denotes a cell that is entirely filled by the liquid phase. Additionally, the model assumes that the transition between the liquid and vapor phases takes place at the saturation temperature.

Continuity equation

$$\frac{\partial(\alpha_v \rho_{v)}}{\partial t} + \nabla.(\alpha_v \rho_v \vec{v}) = S_M \tag{2}$$

here, α_v represents the volume fraction of the vapor phase, ρ_v denotes the density of the vapor phase, and S_M corresponds to the source term for mass.

Momentum equation

Momentum conservation is simulated using the following formulation [3]:

$$\frac{\partial}{\partial t}\left(\rho\vec{v}\right) + \nabla\cdot\left(\rho\vec{v}\vec{v}^{T}\right) = -\nabla P + \nabla.\left[\mu\left(\nabla\vec{v} + \nabla\vec{v}^{T}\right)\right] + \rho\vec{g} + \vec{F}_{CSF} \tag{3}$$

where P refers to the local pressure, $\vec{g}$ represents gravitational

acceleration, and μ denotes the dynamic viscosity.

$$\mu = \alpha_v \mu_v + (1-\alpha_v)\mu_L \quad (4)$$

The term $\vec{F}_{CSF}$ in Eq. (3) refers to the surface tension force per unit volume, determined as a source term via the continuum surface force (CSF) model introduced by Brackbill et al. [12]. This term can be written as:

$$\vec{F}_{CSF} = 2\sigma_{lv}\left(\frac{\alpha_L \rho_L \kappa_v \nabla \alpha_v + \alpha_v \rho_v \kappa_L \nabla \alpha_L}{(\rho_L + \rho_v)}\right) \quad (5)$$

where κ_v and κ_L denote the surface curvatures of the vapor and liquid phases, respectively [12], and σ_{lv} represents the coefficient of surface tension between the liquid and vapor phase.

Energy equation

The energy equation in the VOF formulation is represented in the following manner [13]:

$$\frac{\partial}{\partial t}(\rho C_p T) + \nabla.\left[\vec{v}(\rho C_p T + P)\right] = \nabla.(k \nabla T) + S_E \quad (6)$$

where S_E denotes the energy source term. Furthermore, both the density ρ and the thermal conductivity k are computed as volume-averaged parameters using the respective expressions:

$$\rho = \alpha_v \rho_v + (1-\alpha_v)\rho_L \quad (7)$$

$$k = \alpha_v k_v + (1-\alpha_v)k_L \quad (8)$$

Phase change model

To include the transfer of mass and energy throughout the phase transition between evaporation and condensation, the source terms in the mass conservation equation (Eq. 2) and the energy conservation equation (Eq. 5) are computed using the empirical formulas suggested by Lee [14] and De Schepper et al. [15].

The source terms for mass are computed using the following expressions during the evaporation process:

$$\text{Liquid phase: } S_M = -\beta_e \alpha_l \rho_l \left|\frac{T_{mix} - T_{sat}}{T_{sat}}\right| \quad (9)$$

$$\text{Vapor phase: } S_M = \beta_e \alpha_l \rho_l \left|\frac{T_{mix} - T_{sat}}{T_{sat}}\right| \quad (10)$$

The source terms for mass are computed using the following expressions during the condensation process:

$$\text{Liquid phase: } S_M = \beta_c \alpha_v \rho_v \left|\frac{T_{mix} - T_{sat}}{T_{sat}}\right| \quad (11)$$

$$\text{Vapor phase: } S_M = -\beta_c \alpha_v \rho_v \left|\frac{T_{mix} - T_{sat}}{T_{sat}}\right| \quad (12)$$

The energy source term for the evaporation process is calculated as specified below:

$$\text{Liquid phase: } S_E = -\beta_e \alpha_l \rho_l \left|\frac{T_{mix} - T_{sat}}{T_{sat}}\right| .LH \quad (13)$$

The energy source term for the condensation process is calculated as illustrated here:

$$\text{Vapor phase: } S_E = \beta_c \alpha_v \rho_v \left|\frac{T_{mix} - T_{sat}}{T_{sat}}\right| .LH \quad (14)$$

Equations (8) through (13) utilize T_{mix} to denote the temperature that is volume-averaged based on the mass distribution among the different phases within a computational cell. T_{sat} corresponds to the saturation temperature specific to the operational fluid present within the system. The symbol L_H, as mentioned in Equations (12) and (13), refers to the latent heat associated with the working fluid. Furthermore, the parameters β_e and β_c are relaxation factors that regulate the rate of mass transfer during the evaporation and condensation processes, respectively.

2.4. Validation of the model

In this study, the numerical model has been validated by comparing its results to the experimental data reported by Tang et al. [6] for a grooved heat pipe. The choice to use their experimental findings is based on the similarity between the geometry employed in their study and the one utilized in the present work. The experiment conducted by Tang et al. [6] involved a 19 cm long heat pipe featuring 50 longitudinal grooves. The evaporator section was maintained at a constant temperature boundary condition, while the condenser section had a convective heat transfer boundary condition. The comparison between the experimental data and the numerical investigation carried out in this paper is presented in Fig. 2-a. As shown in the figure, the temperature along the length of the grooved heat pipe wall, as determined by the current numerical method, matches closely with the experimental outputs reported from Tang et al. [6]. An additional validation has been carried out to evaluate the accuracy of the present numerical method. Figure 2-b compares the variations of the thermal resistance in the evaporator section as a function of heat input power. The results obtained from the present numerical method are compared against the experimental data reported by Jafari et al. [16] for a two-phase closed-loop thermosyphon with a filling ratio of 35%. As shown, the numerical results closely match the experimental findings.

3. Results and discussion

In this part, the study presents the outcomes obtained for both the MGHP and ungrooved heat pipe configuration under the condition of a constant temperature applied to the evaporator section. Fig. 3 illustrates a comparison of the water volume fraction between grooved and ungrooved geometries for a specific case with T_e (temperature of the evaporator section) set at 340 K and h_c (forced convection htc for the condenser surrounding) at 300 W m-2 K-1. The contours displayed in this figure provide a visual representation of the water volume fraction distribution, highlighting the effectiveness of the grooved heat pipe in supplying the evaporator part with liquid. The figure reveals that in the grooved case, the liquid film develops within the grooves and extends throughout the adiabatic and evaporation sections of the heat pipe. This indicates that the grooves facilitate the transportation of liquid to the evaporator section. On the other hand, for the ungrooved case, the liquid films dry out before reaching the evaporation section within 10 seconds. This suggests that without the grooves, the liquid supply to the evaporator is insufficient, leading to a higher likelihood of dry-out and reduced heat transfer efficiency.

Volume fraction distribution for grooved and ungrooved cases are compared in Fig. 4. The ungrooved heat pipe has a uniform water volume fraction over its entire length, but the value for the water volume fraction of the MGHP demonstrates a sharp increase at the beginning of the heat pipe and decreases slowly towards the end of the condenser section. Also, the overall liquid volume fraction of the grooved case is up to 100% higher than that of the ungrooved one. This discrepancy indicates that the grooved heat pipe exhibits superior thermal performance relative to the ungrooved heat pipes. This may be attributed to a stronger capillary drive force within the grooved heat pipe. Besides, the increased surface area of the heat transfer is an important contributing factor to the enhancement of the heat transfer in the MGHP.

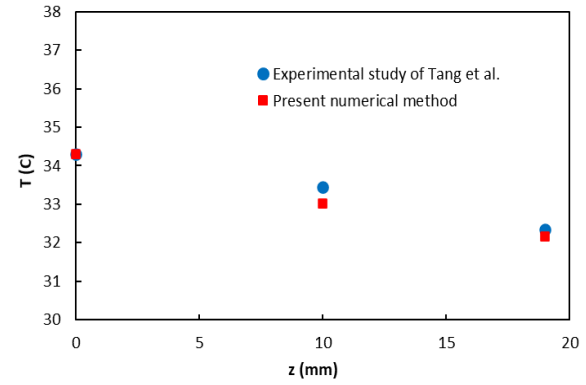

(a)

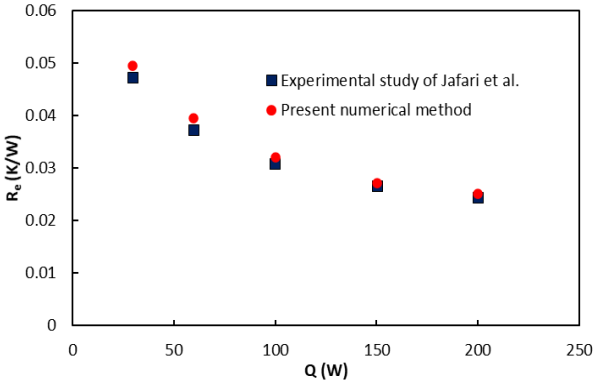

(b)

Fig. 2 Comparison of the numerical results obtained by the present method with experimental data: (a) Grooved heat pipe wall temperature distribution along the axis from Tang et al. [6] (b) Variations of evaporator thermal resistance with heat input power from Jafari et al. [16].

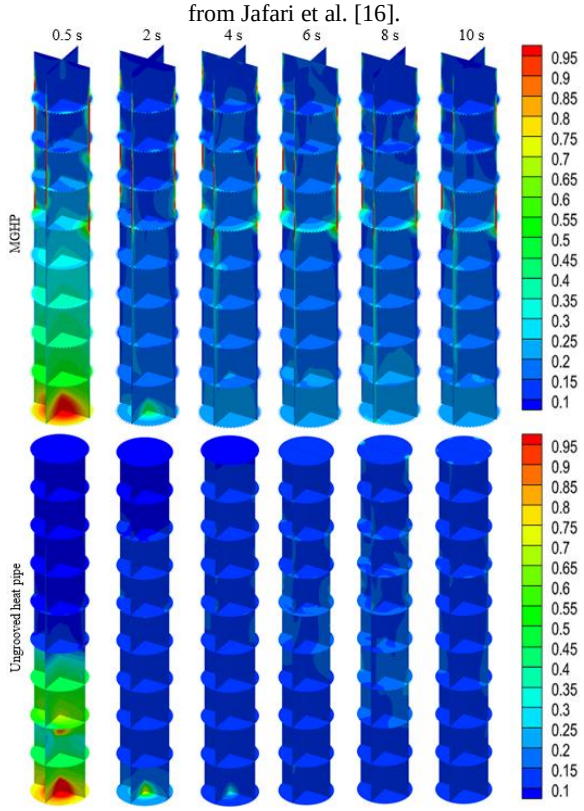

Fig. 3 Water volume fraction comparison for grooved and ungrooved heat pipes at Te=340 K, h=300 Wm-2K-1.

Fig. 5 demonstrates the water volume fraction contours for all the grooved cases with same condenser HTC but different temperatures applied at the evaporator for t=10 s. It's clear that by increasing the input temperature, the liquid films become thinner, but at all cases the condensate liquid flowback to the evaporator is sufficient, and the evaporator doesn't reach the dry-out condition. Fig. 6 illustrates the water volume fraction contours for the cases that have the same input temperature for t=10 s, but have different condenser HTCs. It is apparent from the figure that, despite the variations in condenser HTCs, all cases exhibit a consistent and adequate liquid flowback to the evaporator section. This indicates that the system's design effectively supports the return of liquid to the evaporator, ensuring continuous operation and stability, even under differing heat transfer conditions. The presence of sufficient liquid flowback is critical for maintaining the efficiency of the thermal management system, as it ensures that the evaporator is adequately supplied with liquid, thereby preventing dry-out and optimizing heat removal.

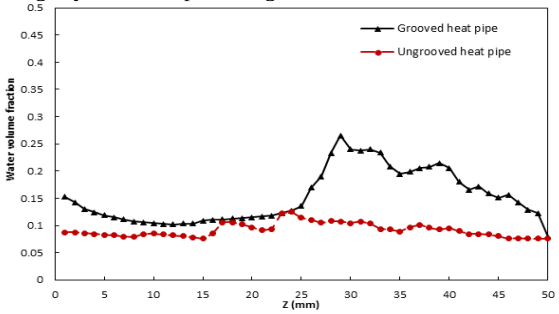

Fig. 4 Water Volume fraction for Grooved and ungrooved heat pipes at T_e=340 K and h_c=300 $Wm^{-2}K^{-1}$.

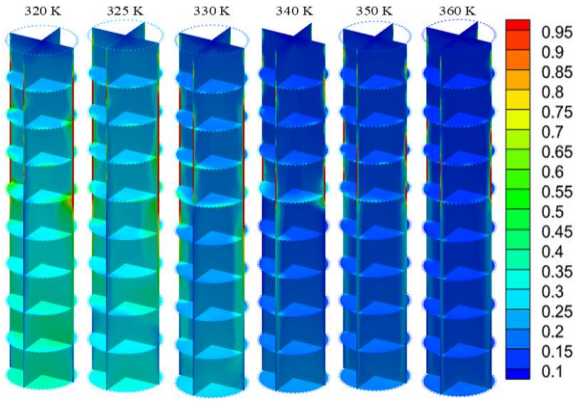

Fig. 5 Liquid phase volume fraction, for the MGHP under h_c=300 W m^{-2} K^{-1} and different evaporator temperature values at t=10 s

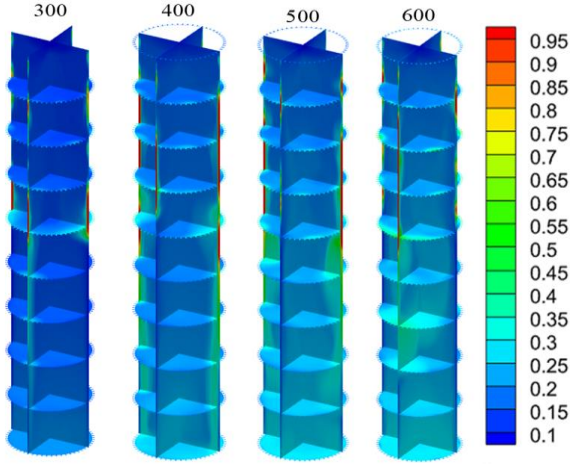

Fig. 6 Liquid phase volume fraction, for the MGHP under T_e=340 K and different HTCs of the condenser at t=10 s.

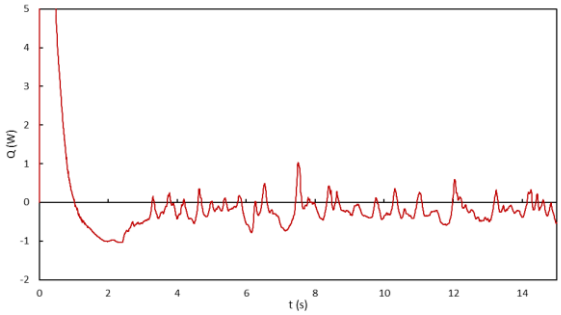

Fig. 7 Net heat transfer rate for T_e=340 K and h_c=300 $Wm^{-2}K^{-1}$.

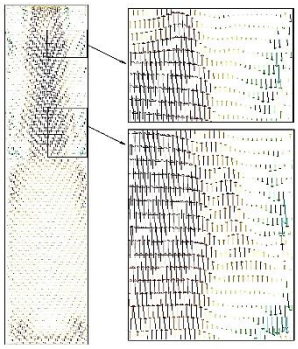

Fig. 8 The velocity vectors of the grooved heat pipe at T_e=340 K and h_c=300 $Wm^{-2}K^{-}$

Fig. 7 demonstrates the net heat transfer rate of the MGHP over time. It can be seen that the MGHP has reached thermal equilibrium after 4 s, only having small fluctuations. These fluctuations depend on many variables including the working fluid and the geometry and their value can be higher or lower. The magnitude of these fluctuations can vary depending on these variables, potentially resulting in higher or lower oscillations in different configurations. The ability of the MGHP to achieve thermal equilibrium relatively quickly, despite these minor fluctuations, underscores its efficiency and stability in managing heat transfer in thermal systems. Fig. 8 demonstrates the velocity vectors for an MGHP. As can be see, the flow direction near the edges and inside the grooves is downwards. Due to capillary drive and gravitational pull, the condensate liquid forms at the condenser section, and starts flowing towards the evaporator end. The grooves are adequately supplying evaporator with liquid and keep heat pipe from reaching the dry-out condition. As mentioned before, the increased surface area of the heat transfer and the enhanced capillary pressure inside the grooves, are the main factors improving the overall thermal performance of the MGHP in comparison with an ungrooved heat pipe.

Fig. 9 (a-f) depicts the wall temperature distribution along the MGHP. It is shown that the MGHP reaches a stable operating condition after t=4 s and the wall temperature profiles remain unchanged after that. This is mainly because of the grooved heat pipe's ability to return an appropriate and adequate quantity of the condensed liquid returned to the evaporator part.

Fig. 10 demonstrates the heat transfer rate of the evaporator section for various input temperatures and compares grooved and ungrooved heat pipes. It is evident that the heat transfer rate of the MGHP is substantially higher than the ungrooved case. As illustrated in Fig. 11, the heat transfer rate for every given input temperature is significantly higher for the grooved heat pipe. the average heat transfer rate for all different evaporator temperatures is quite higher for the MGHP in comparison to the ungrooved geometry. Also, it can be seen that for the heat transfer rate averaged over 10-15s that corresponds to a stable working condition, the heat transfer rate at evaporator section is almost the same for all evaporator temperatures.

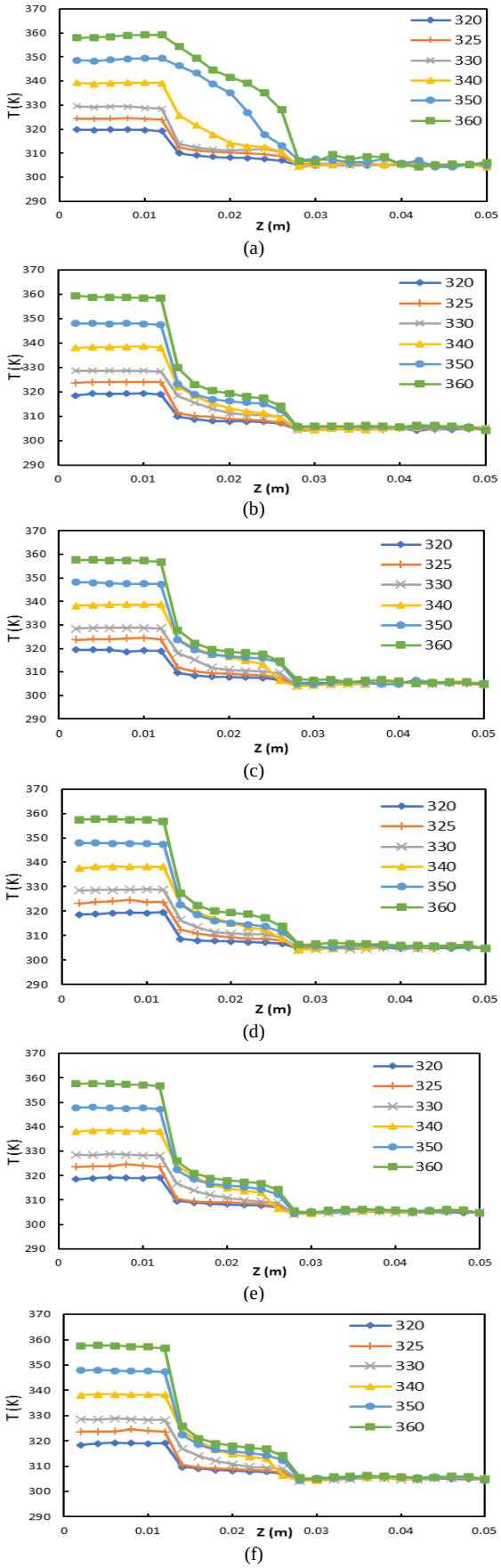

Fig. 9 Wall temperature distribution along the grooved heat pipe: a) 2 s, b) 4 s, c) 6 s, d) 8 s, e) 10 s, f)12 s

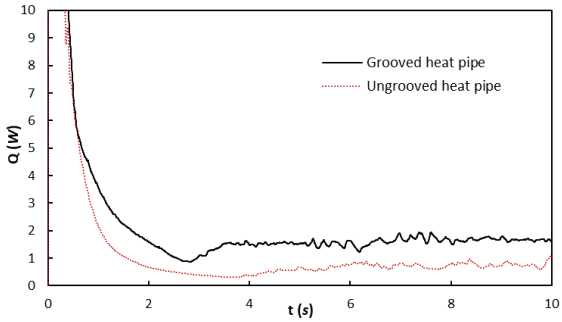

Fig. 10 Evaporator heat transfer rate for T_e=350 K,h_c=300 $Wm^{-2}K^{-1}$

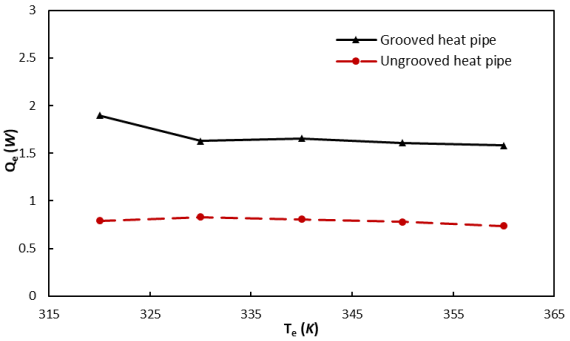

Fig. 11 Evaporator heat transfer rate averaged over 10-15s

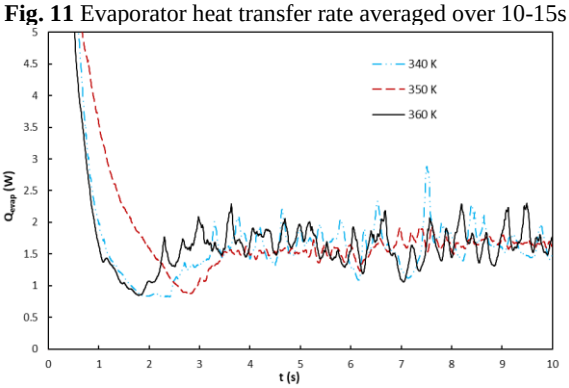

Fig. 12 Heat transfer rate comparison for T_e=330 K, 340 K and 350 K at h_c=300 $Wm^{-2}K^{-}$

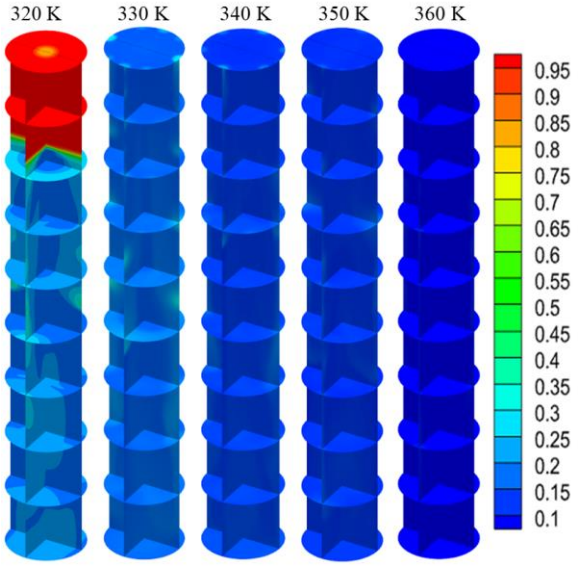

Fig. 13 Liquid phase volume fraction, for the ungrooved heat pipe under h_c=300 W m^{-2} K^{-1} and different evaporator temperature values at t=10s

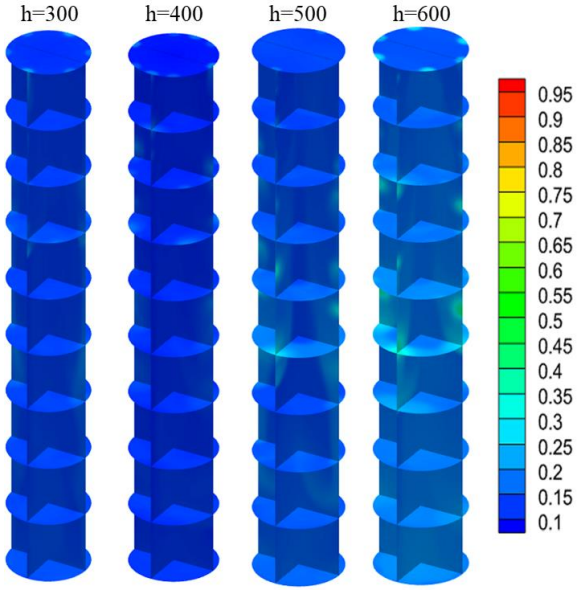

Fig. 14 Liquid phase volume fraction, for the MGHP under T_e=340 K and different HTCs of the condenser at t=10 s

Fig. 12 demonstrates a comparison of the heat transfer rate among three different input temperature of 340, 350 and 360 K. It's clear that the case with the highest temperature reaches a stable thermal performance faster than the other two cases.

Fig. 13 and Fig. 14 illustrate the water volume fraction for the ungrooved heat pipe for different evaporator temperatures at h_c=300 W m*2 K-1 and for different condenser coefficients at T_e=340 K respectively. It is clear that at T_e=320 K the condenser is condensing more liquid than the evaporator can vaporize, but due to insufficient capillary force, a significant portion of the condensate liquid accumulates and overwhelms the condenser section. On the other hand, at temperatures higher than 330 K, the condenser is unable to match the rate at which the evaporator is vaporizing the liquid and thus, the heat pipe has reached the dry-out conditions. Also, the contours at Fig. 14 clearly depict that the ungrooved heat pipe can reach thermal equilibrium under T_e=340 K only if we raise the HTC applied to the condenser by 66%, to a value of 500 W m-2 K-1. By increasing the HTC to h_c=600 W m-2 K-1, we can see that the ungrooved heat pipe has a good water volume fraction present at the evaporator section.

4. Conclusion

This study provides a comprehensive comparison of the thermal performance of micro-grooved and ungrooved heat pipes under varying evaporator temperatures and condenser heat transfer coefficients (HTCs). The results demonstrate that the introduction of rectangular grooves in the heat pipe significantly enhances thermal performance. Specifically, the grooved heat pipe exhibited nearly double the heat transfer rate compared to the ungrooved counterpart. Two primary factors contribute to this improvement: the increased heat transfer surface area due to the grooves and the enhanced capillary force that promotes more efficient liquid flowback from the condenser to the evaporator. These findings suggest that incorporating grooves in heat pipe design can dramatically increase their thermal capacity and efficiency. The implications of these results are significant for future heat pipe designs, particularly in applications requiring efficient thermal management in compact spaces, such as in electronics cooling or energy systems. The enhanced performance of grooved heat pipes opens up opportunities for optimizing thermal regulation in various high-performance environments, paving the way for more effective and reliable heat management solutions.

References

[1] G. Rouaze, J. B. Marcinichen, F. Cataldo, P. Aubin, and J. R. Thome, "Simulation and experimental validation of pulsating heat pipes", Applied Thermal Engineering, vol. 196, 2021.

[2] A. M. Al Jubori and Q. A. Jawad, "Computational evaluation of thermal behavior of a wickless heat pipe under various conditions", Case Studies in Thermal Engineering, vol. 22, 2020.

[3] A. Tarokh, C. Bliss, and A. Hemmati, "Performance enhancement of a two-phase closed thermosyphon with a vortex generator", Applied Thermal Engineering, vol. 182, 2021.

[4] J. Jose and T. K. Hotta, "Numerical investigation on thermal performance of nanofluid-assisted wickless heat pipes for electronic thermal management", Journal of Thermal Science and Engineering Applications, vol. 16, 2024.

[5] A. A. Abdulshaheed, P. Wang, G. Huang, Y. Zhao, and C. Li, "Filling ratio optimization for high-performance nanoengineered copper-water heat pipes", Journal of Thermal Science and Engineering Applications, vol. 13, 2021.

[6] Y. Tang, Z. Hu, J. Qing, Z. Xie, T. Fu, and W. Chen, "Experimental investigation on isothermal performance of the micro-grooved heat pipe", Experimental Thermal and Fluid Science, vol. 47, pp. 143–149, 2013.

[7] J. Cheng, G. Wang, Y. Zhang, P. Pi, and S. Xu, "Enhancement of capillary and thermal performance of grooved copper heat pipe by gradient wettability surface", International Journal of Heat and Mass Transfer, vol. 107, pp. 586–591, 2017.

[8] T. Naemsai, N. Kammuang-lue, P. Terdtoon, and P. Sakulchangsatjatai, "Numerical model of heat transfer characteristics for sintered-grooved wick heat pipes under non-uniform heat loads", Applied Thermal Engineering, vol. 148, pp. 886–896, 2019.

[9] A. Gomaa, W. Ahmed Rady, A. Z. Youssef, and A. M. Elsaid, "Thermal performance of heat pipe at different internal groove ratios and working fluids: An experimental investigation", Thermal Science and Engineering Progress, vol. 41, 2023.

[10] H. Alijani, B. Çetin, Y. Akkuş, and Z. Dursunkaya, "Experimental thermal performance characterization of flat grooved heat pipes", Heat Transfer Engineering, vol. 40, pp. 784–793, 2019.

[11] F. Yao, C. Yu, X. Li, and C. Shen, "Numerical study on the heat transfer characteristics of axially grooved heat pipe assisted by gravity", Microgravity Science and Technology, vol. 33, 2021.

[12] J. U. Brackbill, D. B. Kothe, and C. Zemach, "A continuum method for modeling surface tension", Journal of Computational Physics, vol. 100, pp. 335–354, 1992.

[13] J. Anderson, Computational Fluid Dynamics: The Basics with Applications, McGraw-Hill, 1995.

[14] W. H. Lee, "Pressure iteration scheme for two-phase flow modeling", Multiphase Transport: Fundamentals, Reactor Safety, Applications, vol. 1, pp. 407–431, 1980.

[15] S. C. K. De Schepper, G. J. Heynderickx, and G. B. Marin, "Modeling the evaporation of a hydrocarbon feedstock in the convection section of a steam cracker", Computers and Chemical Engineering, vol. 33, pp. 122–132, 2009.

[16] D. Jafari, P. Di Marco, S. Filippeschi, and A. Franco, "An experimental investigation on the evaporation and condensation heat transfer of two-phase closed thermosyphons", Experimental Thermal and Fluid Science, vol. 88, pp. 111–123, 2017.